CHAPTER SEVENTEEN

Optical Melting Measurements of Nucleic Acid Thermodynamics

Susan J. Schroeder* *and* Douglas H. Turner†

Contents

Abstract

Optical melting experiments provide measurements of thermodynamic parameters for nucleic acids. These thermodynamic parameters are widely used in RNA structure prediction programs and DNA primer design software. This review briefly summarizes the theory and underlying assumptions of the method and provides practical details for instrument calibration, experimental design, and data interpretation.

1. Introduction

A theory is the more impressive the greater the simplicity of its premises is, the more different *[sic]* kinds of things it relates, and the more extended is its area of applicability. Therefore, the deep impression which classical

* Department of Chemistry and Biochemistry, University of Oklahoma, Norman, Oklahoma, USA
† Department of Chemistry, University of Rochester, Rochester, New York, USA

Methods in Enzymology, Volume 468
ISSN 0076-6879, DOI: 10.1016/S0076-6879(09)68017-4

> thermodynamics made upon me. It is the only physical theory of universal content concerning which I am convinced that, within the framework of the applicability of its basic concepts, it will never be overthrown.
>
> Albert Einstein (Einstein, 1970)

Nucleic acid folding is one area where the basic concepts of thermodynamics have found wide ranging applicability. RNA thermodynamic parameters have applications to diverse areas of study such as rhinovirus evolution and recombination (Palmenberg *et al.*, 2009) antisense therapeutics, for example, Vitravene, which is the first FDA-approved nucleic acid therapeutic and which targets cytomegalovirus in the human eye (Anderson *et al.*, 1996) models of the HIV-1 RNA structural elements (Parisien and Major 2008; Wilkinson *et al.*, 2008) cancer microRNA target specificity (Doench and Sharp, 2004); the mechanisms of RNA interference (Ameres *et al.*, 2007); the mechanism of group I introns (Bevilacqua and Turner, 1991; Narlikar *et al.*, 1997; Pyle *et al.*, 1994); the discovery of noncoding RNAs in genomes (Uzilov *et al.*, 2006; Washietl *et al.*, 2005); and tRNA codon recognition in protein translation (Ogle *et al.*, 2002). In principle, thermodynamics can predict the populations of structures that would be present at equilibrium, although the current knowledge of the sequence dependence of nucleic acid thermodynamics limits the accuracy of such predictions. Much of the known thermodynamics has been measured by optical melting, which has several advantages over the more accurate calorimetric methods. Relatively small quantities of sample are required; the experiments are fast; and the instrumentation is relatively inexpensive. For example, if two 8-mer RNA oligonucleotides with internal loops are predicted to have different stabilities, with only approximately 1 μmol of each RNA and one day of optical melting experiments by a hard-working student, one can determine which internal loop is more thermodynamically stable. (Very few bets in the RNA world can be resolved so quickly!) This chapter provides details on the optical melting methods used most often, and includes both technical aspects and a discussion of the assumptions in interpretation.

2. Instrumentation

UV spectrometers suitable for optical melting experiments are commercially available from Beckman, Cary, and Shimadzu corporations. The primary requirements in a UV spectrometer are good optics; accurate, variable temperature control; and a cell holder for several small cuvettes. This article will discuss details of the Beckman DU800 spectrometer, but the general principles apply to all UV spectrometers. The Beckman DU800 spectrometer specifications for temperature are ± 1 °C from 20 to 60 °C

with the DU800 high-performance temperature controller unit, although the instrument range is 13–95 °C. A customized cell holder with chilled water circulation to remove heat from the peltier-controlled cell holder allows accurate ±1 °C temperature control to 0 °C. Dry air or nitrogen gas flowing through the cell chamber prevents condensation on the cells at low temperatures. The microcell holder contains places for six cuvettes and uses the cell transporter unit. Standard Beckman cells have a 1 cm pathlength and a 400 μL volume. Custom quartz cells with pathlengths of 0.1 cm, 0.5 cm, 1.0 cm and volumes of 40 μL, 200 μL, and 400 μL, respectively, in dimensions that fit into the Beckman cell holder can be obtained from Hellma, Inc. and NSG Precision Cells.

3. Calibrations

The Beckman DU800 spectrometer software automatically runs several initialization calibration tests when the instrument is turned on. These tests are run with no samples in the instrument and the lid closed. The initialization tests check the gain, the visible lamp, the light path, the shutter, the filter, the wavelength drive, and the detector performance. Turn the instrument power off when not in use, so that these calibrations are automatically checked every time the instrument is used. In addition, the performance validation tests following the manufacturer's instructions should be run monthly to insure reliable instrument performance. The performance validation checks the wavelength accuracy (±0.2 nm); wavelength repeatability (±0.1 nm); resolution (<1.80 nm); baseline flatness (<0.0010 A); noise at 500 nm (<0.000200 A); and stability at 340.0 nm for 60 min (<0.0030 A drift). ("A" is a unit of absorbance defined by the NIST 930D solid filter at 546 nm.) Additional checks for temperature, absorbance, pathlength, and cell holder alignment can be done manually at installation and as necessary during use.

The temperature can be manually tested with a microprobe, such as the Ertco-eutechnics digital thermometer model 4400. Test the accuracy of the microprobe thermometer in a water bath and compare with an accurate mercury thermometer. Fill six 1-cm cuvettes with double distilled water and seal five cuvettes with Teflon tape and stoppers. Insert the temperature probe into one of the cuvettes and seal with the small stopper around the probe. Check that the probe is directly upright in the cell and does not touch the sides of the cuvette. Keep the lid closed as much as possible while measuring temperature. The temperature of the cell holder can be manually set, and the actual temperature recorded by the software appears in the lower right hand corner of the screen. Check that the temperature is within ±1 °C at all cell positions at several temperatures, for example, 5, 15, 25, 35,

45, and 55 °C. Allow approximately 5 min for equilibration at each temperature. When checking the temperature at higher than 60 °C, take care to note any water evaporation. The temperature measurement will not be accurate if the cell is not full of water. Then check the temperature as if a melting experiment were being run with a heating rate of 0.5 or 1 °C per minute from 0 to 90 °C. Check the temperature in one of the first three and in one of the last three cell positions to insure that the peltier devices embedded in the bottom of the cell holder are accurately matched. The nitrogen flow, the chilled water flow, and the rate of heating can be adjusted so that the actual temperature of the cell matches the recorded temperature. Alternatively, temperature offsets can be included in the data analysis if there is a reproducible difference in temperature between cells, although this is not recommended.

The wavelength accuracy can be measured using a holmium oxide filter in place of the cell holder and scanning wavelength from 200 to 800 nm at a rate of 1200 nm/min. The shape and position of the peaks are the important features of the spectrum rather than the exact intensities. There should be three strong distinct peaks between 440 and 460 nm. Peaks should be clearly distinguished at 241.5, 279.3, 287.6, 333.8, 360.8, 385.8, 418.5, 453.4, 459.9, 536.4, and 637.5 ± 0.2 nm (Allen, 2007). Any peaks appearing below 225 nm indicate stray light in the instrument. If this scan does not show the appropriate peaks, then replace the UV bulb following the manufacturer's instructions or troubleshoot other possible problems in the optics.

The absorbance may be checked by measuring the absorbance of a known stock solution, such as 0.00400 g/L of $K_2Cr_2O_7$ in 0.05 *M* KOH, referenced to a 0.05 *M* KOH solution at 25 °C. (Table 17.1) (Gordon and Ford, 1972). Measure the same sample in the same cell in each cell position to check the cell holder alignment. If the absorbance varies more than ±0.0005 A at different cell positions, then rerun the transporter alignment with no samples in the cell holder. The service

Table 17.1 Absorbance for 0.00400 g/L of $K_2Cr_2O_7$ in 0.05 *M* KOH[a]

λ (nm)	*A*	λ (nm)	*A*	λ (nm)	*A*
220	0.446	315	0.046	400	0.396
230	0.171	330	0.149	420	0.124
240	0.295	340	0.316	440	0.054
250	0.496	350	0.559	460	0.018
260	0.633	360	0.830	480	0.004
275	0.757	370	0.987	500	0.000
290	0.428	375	0.991		
300	0.149	390	0.695		

[a] Values are from Gordon and Ford (1972).

diagnostics calibrations can be run by a Beckman service technician to correct the alignment. Use the same solution with a known absorbance in cells of each pathlength and verify the pathlength accuracy using Beer's Law:

$$A = \varepsilon c l \tag{17.1}$$

where A is absorbance; ε is the extinction coefficient; c is concentration; and l is the pathlength.

4. Brief Theory of Optical Melting Experiments

In principle, optical melting curves could be analyzed by a partition function approach in which every base pair is considered separately. This approach, however, would require a global fit of melting data for many sequences and refitting the data when additional sequences are added. Therefore, data are typically analyzed with a two-state model, which assumes that each strand is either completely paired or unpaired. The equilibrium for duplex formation is represented as either a self-complementary or non-self-complementary association (Cantor and Schimmel, 1980; Turner, 2000):

$$2\mathrm{A} \leftrightarrow \mathrm{A}_2 \tag{17.2}$$

$$\mathrm{B} + \mathrm{C} \leftrightarrow \mathrm{B{\cdot}C} \tag{17.3}$$

The equilibrium for a unimolecular transition, for example, a hairpin, is represented as:

$$\mathrm{D} \leftrightarrow \mathrm{E} \tag{17.4}$$

For self-complementary (Eq. (17.2)) or non-self-complementary equilibria (Eq. (17.3) with equal concentrations of B and C), the equilibrium constant is given by:

$$K = (\alpha/2)/(C_\mathrm{T}/a)(1-\alpha)^2 \tag{17.5}$$

C_T is the total strand concentration:

$$C_\mathrm{T} = [\mathrm{A}] + 2[\mathrm{A}_2] \quad \text{self-complementary} \tag{17.6}$$

$$C_\mathrm{T} = [\mathrm{B}] + [\mathrm{C}] + 2[\mathrm{B{\cdot}C}] \quad \text{non-self-complementary} \tag{17.7}$$

"a" has a value of 1 for self-complementary duplexes and 4 for non-self-complementary duplexes. α is the fraction of strands in a duplex. For a unimolecular transition,

$$K = \alpha/(1-\alpha) = [\mathrm{E}]/[\mathrm{D}] \tag{17.8}$$

where

$$\alpha = [\mathrm{E}]/([\mathrm{D}] + [\mathrm{E}]) \tag{17.9}$$

Figure 17.1 shows data for the non-self-complementary duplex, 5′-GAGC**GA**CGAC-3′/3′-CUCG**AAG**GCUG-5′. At low temperatures, the strands are in a duplex and the absorbance is low. As the temperature is increased, the duplex dissociates into single strands. The total concentration of strands can be measured using the absorbance at 80 °C and the extinction coefficient for that sequence. The difference in absorbance between duplex and single strands is the hyperchromicity. For self-complementary or non-self-complementary duplexes with equal concentrations of each strand, the melting temperature, T_M, in kelvins or T_m in degrees Celsius, is the point at which the concentrations of strands in duplex and in single strands are equal. The steepness of the transition indicates the cooperativity of the transition. The width and maximum of first derivative of the melting curve can also indicate the cooperativity and melting temperature, although the peak of the derivative curve only occurs at the T_M when the transition is unimolecular (Gralla and Crothers, 1973; Marky and Breslauer, 1987). T_M is most accurately measured by fitting the lower and upper baselines. The melting temperature is measured at several concentrations over a 100-fold range and then plotted versus the concentration in a van't Hoff plot. The van't Hoff equation relates the melting temperature in kelvins (T_M), total strand concentration (C_T), enthalpy (ΔH^o), and entropy (ΔS^o):

$$1/T_M = (R/\Delta H^o)\ln(C_T/a) + \Delta S^o/\Delta H^o \tag{17.10}$$

where R is the ideal gas constant, 1.987 cal K^{-1} mol^{-1} or 8.3145 J K^{-1} mol^{-1}. The slope of the van't Hoff plot gives the enthalpy change, and the y-intercept gives the ratio of entropy change to enthalpy change. The free energy and equilibrium constant at any temperature can then be calculated using Gibb's relation:

$$\Delta G^o = \Delta H^o - T\Delta S^o, \quad K = e^{-\Delta G^o/RT} \tag{17.11}$$

The errors in enthalpy and entropy changes are typically around 10%. Because these errors are correlated, the errors in free energy change are typically 2%.

The melting curve can be fit using Meltwin software (McDowell and Turner, 1996), although other software is available to perform the same mathematical analysis (Draper *et al.*, 2001; Siegfried and Bevilacqua, 2009). The Meltwin software uses seven parameters to fit each curve (Fig. 17.1): the total strand concentration, enthalpy and entropy changes of the transition, the slope and intercept of the lower baseline (double-stranded region), and the slope and intercept of the upper baseline (single-stranded region). The total strand concentration is the only nonfloating parameter and is determined at a high-temperature absorbance point. A Marquardt–Levenberg

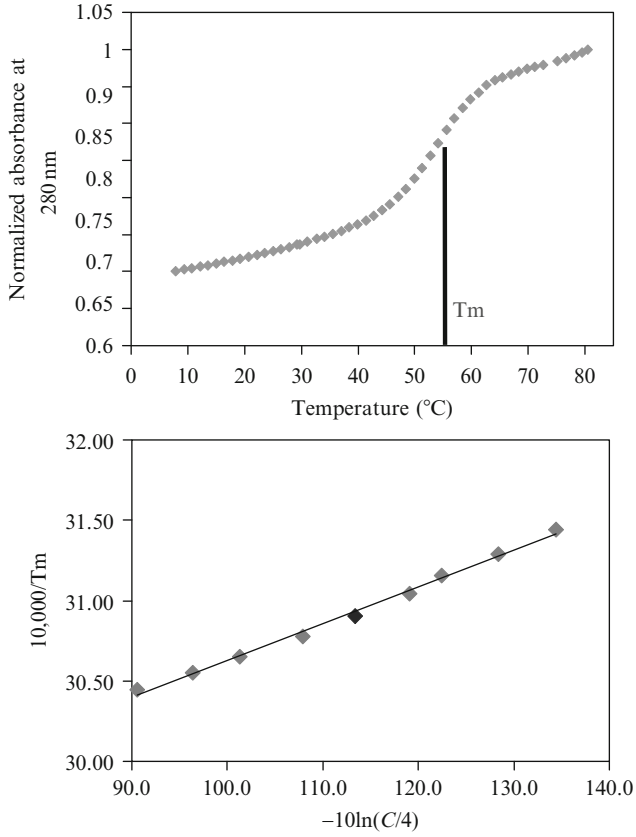

Figure 17.1 Optical melting data. The normalized UV absorbance (280 nm) versus temperature (°C) curve (top). Van't Hoff plot (bottom): $1/T_M$ versus ln (C_T/a).

fitting routine is applied to each curve to find the best parameter values. The parameters and fitting follow an Ising model:

$$A_T = (1 - \alpha)A_{RC} + \alpha A_{ST} \tag{17.12}$$

where A_T is the total absorbance, A_{RC} is the absorbance of the random coil or single strands, A_{ST} is the absorbance of the stacked duplex, and α is the fraction of strands in the duplex conformation. The truncation points for the fitting can be selected by the user. It is important to have enough points in the upper and lower baselines to find a good fit, although with a low T_m the points in the lower baseline may be few in practice. At higher temperatures, it is important to avoid evaporation effects, which cause the absorbance to appear higher than true values, and to exclude such points from the fit. The position of the truncation points of the fit can have a significant impact on the values of the enthalpy parameter.

5. Two-State Assumption

An important assumption in the analysis described above is that only two states exist for the RNA: single strands or duplex. Any intermediates between these two conformations are assumed to be at very low concentration and not to contribute significantly to the absorbance. Also, the duplex must fold into a single conformation with no alternative folds. If the values for the enthalpy change calculated according to the fit of the melting curves and the van't Hoff plot agree within 15%, then the results are consistent with the two-state assumption. Although the exact cutoff value for consistent two-state behavior is a matter of debate and interpretation, if the enthalpy values calculated with the two different fitting methods are not consistent, then the analysis does not provide valid thermodynamic parameters.

6. ΔC_p^o Assumption

The above equations neglect the temperature dependence of ΔH^o and ΔS^o, which for a constant heat capacity, ΔC_p^o, is given by:

$$\Delta H^o(\mathrm{T}) = \Delta H^o_{\mathrm{T_o}} + \Delta C_p^o(T - T_o) \tag{17.13}$$

$$\Delta S^o(\mathrm{T}) = \Delta S^o_{\mathrm{T_o}} + \Delta C_p^o \ln(T/T_o) \tag{17.14}$$

Usually, ΔC_p^o will not be zero because stacking in the single strands is temperature dependent (Holbrook *et al.*, 1999). The best way to determine ΔC_p^o is by isothermal titration calorimetry at different temperatures (Diamond *et al.*, 2001; Mikulecky and Feig, 2006). It is sometimes possible, however, to obtain estimates from optical melting data by plotting the fitted values of ΔH^o from individual melting curves versus T_M and the fitted values of ΔS^o versus $\ln T_M$ (Diamond *et al.*, 2001; Petersheim and Turner, 1983). This is best attempted when the ΔH^o is not large so that there is a large concentration-dependence of T_M. In general, however, the experimental errors in optical melting data do not allow accurate determination of ΔC_p^o (Chaires, 1997). Fortunately, the systematic errors in fitting ΔH^o and ΔS^o due to neglecting ΔC_p^o compensate each other so that the ΔG^o is a reliable parameter.

7. Experimental Design

When designing sequences to study the thermodynamic stabilities of different noncanonical RNA motifs, consider carefully the stems' stabilities, the expected T_m, the advantages of non-self-complementary or

self-complementary systems, and possible alternate folds. When choosing stem duplexes for internal or multibranch loop, the predicted thermodynamic stabilities of each stem should be close so that the duplexes unfold in a two-state manner. The predicted T_m of the folded forms should be as close to 37 °C as possible to minimize the extrapolation for calculating ΔG°_{37}. Self-complementary systems have the advantages of simplicity and not requiring determination of oligonucleotide concentrations prior to the melt because mixing of equimolar amounts of two different strands is not required. A self-complementary system also enables incorporation of two motifs in one duplex, thus doubling the effect of the motif. This is particularly useful when the free energy increment of the noncanonical motif is small, such as for dangling ends. While non-self-complementary duplexes require accurately mixing equimolar amounts of two strands, they have the potential to "mix and match" different strands and thus enable a wider sequence diversity within a motif using fewer different sequences.

The possibilities of alternate folds should be considered even for short sequences. Sometimes changing a Watson–Crick base pair distant from the intended noncanonical pair can change the propensity for alternate duplex formation. Prediction programs such as mfold (Zuker, 1989) and RNAstructure (Mathews *et al.*, 2004) can generate some suboptimal folds for both unimolecular and bimolecular folds. A simple graphical method for finding alternate folds is to create a grid as shown in Fig. 17.2. Every possible Watson–Crick pairing is assigned an X, potentially stable noncanonical pairs such as GU can be assigned an O. Possible helices appear as a diagonal line of X's and O's. For example, in the sequence on the left in Fig. 17.2, the intended duplex has two GU pairs at the ends of the helix; the thermodynamic stability of GU is often idiosyncratic and depends on the helix position. The only alternative duplexes have positive predicted free energy and are thus unlikely to form. In contrast, the sequence on the right differs only in the order of the two middle GC pairs, but this slight change creates the possibility for several more stable alternative duplexes. The middle GC pairs are unlikely to affect the measurement of the thermodynamic stability of the terminal GU pairs. Keep in mind that these are predicted free energy values; and the idiosyncratic nature of non-Watson–Crick pairs, such as GU pair stabilities, is the reason to continue measuring thermodynamic parameters with optical melting experiments.

One-dimensional proton NMR of 0.2–1 m*M* RNA in 90% H_2O and 10% D_2O, 100 m*M* NaCl, 10 m*M* phosphate, and 0.5 m*M* Na_2EDTA in a 500 MHz spectrometer is a quick way to check that the expected duplex forms. The extensive dialysis and sample preparation necessary for high-quality 2D NMR spectra is often not necessary for a quick 1D proton spectrum. The correct number and chemical shift of imino protons can verify that the proton spectrum is consistent with the intended duplex design. The imino protons in the pairs at the terminus of a duplex may be

	5′G	U	A	U	**C**	**G**	A	U	G	U
U	O		X			O	X		O	
G		O		O	X			O		O
U	O		X			O	X		O	
A		X		X				X		X
G		O		O	X			O		O
C	X					X			X	
U	O		X			O	X		O	
A		X		X				X		X
U	O		X			O	X		O	
5′G		O		O	X			O		O

5′-GUAUCGAUGU-3′ $\Delta G^\circ = -7.0$ kcal/mol
3′-UGUAGCUAUG-5′

5′-GUAUCGAUGU-3′ $\Delta G^\circ = +0.2$ kcal/mol
3′-UGUACGUAUG-5′

5′-GUAUGCAUGU-3′ $\Delta G^\circ = +1.8$ kcal/mol
3′-UGUACGUAUG-5′

	5′G	U	A	U	**G**	**C**	A	U	G	U
U	O		X		O		X		O	
G		O		O		X		O		O
U	O		X		O		X		O	
A		X		X				X		X
C	X				X				X	
G		O		O		X		O		O
U	O		X		O		X		O	
A		X		X				X		X
U	O		X		O		X		O	
5′G		O		O		X		O		O

5′-GUAUGCAUGU-3′ $\Delta G^\circ = -7.6$ kcal/mol
3′-UGUACGUAUG-5′

5′-GUAUGCAUGU-3′ $\Delta G^\circ = -8.0$ kcal/mol
3′-UGUACGUAUG-5′

5′-GUAUGCAUGU-3′ $\Delta G^\circ = -6.1$ kcal/mol
3′-UGUACGUAUG-5′

Figure 17.2 Plots to facilitate sequence design. The X's represent possible Watson–Crick pairs. The O's represent possible GU pairs. The intended duplex with terminal GU pairs is shown as the central diagonal. Possible alternative duplexes are shown as shorter diagonals. The sequence differences between the left and right examples are highlighted in bold. The predicted free energies at 37 °C of the possible duplexes are calculated according to (Clanton-Arrowood *et al.*, 2008; He *et al.*, 1991; Mathews *et al.*, 1999, 2004; Miller *et al.*, 2008; O'Toole *et al.*, 2005, 2006; Xia *et al.*, 1998). Note that the nearest-neighbor parameter for 5′-GU/3′-UG is known to be context-dependent and shows non-nearest neighbor effects. In this example, the lowest energy possibility for the terminal mismatches was used. The left hand sequence is preferred because the desired pairing is predicted to be considerably more stable than other pairings.

missing or weak due to exchange with water and fraying at the duplex ends. Too many imino protons implies that more than one conformation of the RNA is stable. The imino protons in GC and AU Watson–Crick pairs resonate between 11-13 ppm and 13-15 ppm, respectively. Imino protons in stable mismatches may be protected from exchange with water and then resonate anywhere between 9.5 and 15 ppm depending on the conformation and protonation of the mismatch (Santa Lucia *et al.*, 1991; Schroeder and Turner, 2000). These resonances for non-Watson–Crick pairs can provide strong supporting evidence that different hydrogen-bonded conformations are the basis for the sequence dependence of the thermodynamic stability. For example, wobble GU pairs show imino proton resonances between 10 and 11.5 ppm and a strong NOE between the two imino protons (Schroeder and Turner, 2001).

The buffer used for optical melting experiments is typically 1 *M* NaCl, 10 or 20 m*M* sodium phosphate or sodium cacodylate at pH 7, and 0.5 m*M* Na_2EDTA. One molar NaCl was initially chosen to stabilize short RNA sequences when RNA synthesis was difficult and time-consuming and has become the standard salt concentration. The phosphate or cacodylate buffers maintain a constant pH over a wide temperature range. Because cacodylate anion has an arsenic atom, the buffer can be stored without concerns about bacterial growth. The buffering range of cacodylate is 5.0–7.4 with a pK_a of 6.3. Noncanonical pairs such as $A^+{\cdot}C$ or $C^+{\cdot}C$ are more stable at low pH, and increased stability at low pH provides evidence for the formation of protonated pairs (Santa Lucia *et al.*, 1991). The Na_2EDTA chelates any divalent cations that promote RNA hydrolysis, especially at high temperatures. Other buffers may be used to test the effects of salt on thermodynamic stabilities. A typical buffer that may resemble more physiological salts is 0.15 *M* KCl, 10 m*M* $MgCl_2$, and 20 m*M* sodium cacodylate, pH 7. When using buffers that contain magnesium, however, the samples cannot be diluted and used again for a melt at another concentration because magnesium facilitates hydrolysis at high temperatures.

If a transition is truly two-state, then the thermodynamics should be the same when measured at any wavelength at which the folded and unfolded states have different absorbances (Cantor and Schimmel, 1980). Typically, 260 or 280 nm light is used. For sequences with a high fraction of GC or AU pairs, 280 or 260 nm, respectively, are preferred in order to maximize the hyperchromicity (Fresco *et al.*, 1963). Sometimes local information can be deduced from optical melting curves at other wavelengths. One case is when a nucleotide absorbs outside the region where the rest of the nucleotides absorb. Measurements at 296 nm provide information on global conformation, and the absorption is due to an n to $\pi^\star$ transition (Testa and Gilham, 1993). DNA duplexes with Hoogsteen pairs also have a signature melting profile at 295 nm (Mergny *et al.*, 2005; Miyoshi *et al.*, 2009).

The purity of oligonucleotides for optical melting experiments should be at least 90% as measured by HPLC or by gel electrophoresis on a denaturing gel. The RNA can be diluted to provide 10 concentrations over a 100-fold range. The maximum and minimum accurate absorbance of the Beckman spectrometer is 2.5 and 0.2, approximately a 10-fold range. The use of cuvettes with 0.1 cm and 1.0 cm pathlengths enables another 10-fold range in concentration. A typical RNA duplex concentration range is from 2.5×10^{-4} M to 2.5×10^{-6} M, and concentration ranges from 60-fold to 150-fold are common. Thus, use Beer's Law and the sequence-dependent extinction coefficient to calculate the necessary dilutions of the RNA samples with optical melting buffer (Cantor and Schimmel, 1980). Unless magnesium is used in the buffer, five sample concentrations can be prepared, run in an optical melting experiment, and then diluted and used again in the next optical melting experiment. Signal-to-noise is usually not a consideration with modern spectrophotometers, but if it is, then the optimum absorbance is 0.434 if the noise is not due to statistical fluctuations in the number of photons hitting the detector (shot noise) (Hammes, 1974; Turner, 1986).

8. Data Interpretation

Analysis of optical melting experiments provides thermodynamic parameters for enthalpy, entropy, and free energy changes for duplex formation. Optical melting experiments, however, do not provide definitive information about the duplex structure, hydrogen bonding, or heat capacity. Although pairing patterns are sometimes inferred from the sequence dependence of RNA motifs, NMR or crystallography is required to provide definitive information about the structure of the RNA duplex. For example, hydrogen-bonded GA and GG pairs are relatively stable thermodynamically in certain contexts (Burkard and Turner, 2000; Schroeder and Turner, 2000; Walter *et al.*, 1994; Wu and Turner, 1996); however, a combination of optical melting experiments and NMR spectroscopy was necessary to determine this. As a consequence of these results, when GA or GG pairs have the potential to form in loops, the possibility of forming a GA or GG pair is often invoked to extend empirical rules to thermodynamic stabilities of unmeasured sequences.

Optical melting studies provide estimates of ΔH° and ΔS° and therefore ΔG° on the basis of the two-state model. The most reliable values for ΔG° are those near the melting temperatures of the experiment. Relative stabilities depend not only on melting temperature but also on the enthalpy change. For example, if duplex A and duplex B have melting temperatures of 70 and 60 °C, respectively, then duplex A is more stable at 70 °C if both RNA concentrations

are the same. If the enthalpy of duplex A is larger than the enthalpy of duplex B, however, duplex B may be the more stable duplex at 37 °C. The ΔG^{o} at the temperature of interest is the true measure of relative stability.

9. Error Analysis

There are many possible sources of error in optical melting studies. SantaLucia and Turner (SantaLucia and Turner, 1997) list two sources of random error: (1) signal-to-noise ratio of the absorbance measurements and (2) variations in sample preparation, and four sources of systematic error: (a) incorrect calibration, (b) a non-two-state transition, (c) incorrect choice of baselines, and (d) neglect of ΔC_p^o.

Sampling errors in $1/T_M$ versus ln C_T plots and in fitted data provide measures of the random errors. Equations for calculating sampling error are given by SantaLucia and Turner (1997) and Xia *et al.* (1998). The random errors from $1/T_M$ versus ln C_T plots are typically on the order of 3%, 3%, and 1% for ΔH^o, ΔS^o, and ΔG^o near the T_M, respectively (Xia *et al.*, 1998). Random errors from averaging values from fitting curves are typically two- to threefold larger. In a study of 51 Watson–Crick complementary duplexes, the errors in ΔS^o were about 13% larger than in ΔH^o because the uncertainty in ΔS^o depends on more terms (Xia *et al.*, 1998). The error in ΔG^o is smaller than that in ΔH^o and ΔS^o because the errors in ΔH^o and ΔS^o are highly correlated in a compensating manner. Random errors in T_m are typically 1–2 °C.

The magnitudes of systematic errors are difficult to estimate. Optical melting results from different laboratories provide one measure. For three DNA sequences reported by separate laboratories (Breslauer *et al.*, 1986; SantaLucia *et al.*, 1996; Sugimoto *et al.*, 1996), differences were 6%, 6%, 3%, and 1 °C for ΔH^o, ΔS^o, ΔG^o_{37}, and T_M, respectively (SantaLucia and Turner, 1997). Values of ΔG^o_{50} for four sequences measured by substrate inhibition in a group I ribozyme reaction (Narlikar *et al.*, 1997) differed an average of 8% from those measured by optical melting (Pyle *et al.*, 1994).

When comparing the free energies of two short RNA duplexes, 0.5 kcal/mol is a reasonable rule of thumb for estimating a significant difference in thermodynamic stabilities. The calculated error in duplex free energy is typically ± 0.2 kcal/mol when using Meltwin software. Non-nearest neighbor effects due to the length of the duplex stems or the position of the mismatch in a helix can be approximately 0.5 kcal/mol (Kierzek *et al.*, 1999; Schroeder and Turner, 2000). The rules for predicting thermodynamic stabilities of duplexes include terms with values less than 0.5 kcal/mol, however. These terms are calculated from linear regression analysis of typically 50–200 duplex free energies, and the terms are justified by statistical significance.

10. Summary

Optical melting experiments can provide a large number of thermodynamic measurements from which generalized rules for predicting nucleic acid stabilities can be derived. These thermodynamic measurements and rules form the core of most RNA and DNA structure prediction algorithms. Contrafold (Do *et al.*, 2006), a new algorithm based on computational conditional training methods and databases of known RNA structures (Griffiths-Jones *et al.*, 2003, 2005), calculated base stacking energies with the same rank order as the nearest neighbor parameters measured by optical melting experiments. This result supports the use of thermodynamic parameters and free energy minimization to predict the structure of functional RNA conformations. Thus, thermodynamic analysis and optical melting experiments are useful tools for exploring the unknown landscapes of the RNA world amidst a flood of sequencing information, low free energy valleys, and peaks of activation energies in ribozymes.

ACKNOWLEDGEMENTS

The authors thank Koree Clanton-Arrowood, Nic Hammond, Biao Liu, and Mai-Thao Nguyen for critical reading of the manuscript. We thank all our students who remind us that teaching and learning are a dynamic equilibrium with arrows that go both ways. D. H. Turner is supported by NIH grant #GM22939. S.J. Schroeder is supported by NSF grant #0844913 and grants from the Oklahoma Center for the Advancement of Science and Technology Plant Science Research Program, the Pharmaceutical Research and Manufacturers of America Foundation, and the American Cancer Society Institutional Research Grant to the Oklahoma Health Science Center.

REFERENCES

Allen, D. (2007). Holmium oxide glass wavelength standards. *J. Res. Natl. Inst. Stand. Technol.* **112,** 303–306.

Ameres, S. L., Martinez, J., and Schroeder, R. (2007). Molecular basis for target RNA recognition and cleavage by human RISC. *Cell* **130,** 101–112.

Anderson, K., Fox, M., Brown-Driver, V., Martin, M., and Azad, R. (1996). Inhibition of human cytomegalovirus immediate-early gene expression by an antisense oligonucleotide complementary to immediate-early RNA. *Antimicrob. Agents Chemother.* **40,** 2004–2011.

Bevilacqua, P. C., and Turner, D. H. (1991). Comparison of binding of mixed ribose-deoxyribose analogues of CUCU to a ribozyme and to GGAGAA by equilibrium dialysis: Evidence for ribozyme specific interactions with 2′OH groups. *Biochemistry* **30,** 10632–10640.

Breslauer, K. J., Frank, R., Blocker, H., and Marky, L. A. (1986). Predicting DNA duplex stability from the base sequence. *Proc. Natl. Acad. Sci. USA* **83,** 3746–3750.

Burkard, M. E., and Turner, D. H. (2000). NMR structures of r(GCAGGCGUGC)2 and determinants of stability for single guanosine-guanosine base pairs. *Biochemistry* **39,** 11748–11762.

Cantor, C. R., and Schimmel, P. R. (1980). *Biophysical Chemistry* W.H. Freeman and Company, New York.

Chaires, J. B. (1997). Possible origin of differences between van't Hoff and calorimetric enthalpy estimates. *Biophys. Chem.* **64,** 15–23.

Clanton-Arrowood, K., McGurk, J., and Schroeder, S. J. (2008). 3′-Terminal nucleotides determine thermodynamic stabilities of mismatches at the ends of RNA helices. *Biochemistry* **47,** 13418–13427.

Diamond, J. M., Turner, D. H., and Mathews, D. H. (2001). Thermodynamics of three-way multibranch loops in RNA. *Biochemistry* **40,** 6971–6981.

Do, C., Woods, D., and Batzglou, S. (2006). CONTRAfold: RNA secondary structure prediction without physics-based models. *Bioinformatics* **22,** e90–e98.

Doench, J. G., and Sharp, P. A. (2004). Specificity of microRNA target selection in translational repression. *Genes Dev.* **18,** 504–511.

Draper, D. E., Bukham, Y. V., and Gluick, T. C. (2001). Thermal methods for the analysis of RNA folding pathways. *Curr. Protoc. Nucleic Acid Chem.* **11.3**.

Einstein, A. (1970). Autobiographical Notes on Albert Einstein: Philosopher-Scientist. Cambridge University Press, London.

Fresco, J. R., Klotz, L. C., and Richards, E. G. (1963). A new spectroscopic approach to the determination of helical secondary structure in ribonucleic acids. *Cold Spring Harbor Symp. Quant. Biol.* **28,** 83–90.

Gordon, A., and Ford, R. (1972). *The Chemist's Companion: A Handbook of Practical Data, Techniques, and References* Wiley, New York.

Gralla, J., and Crothers, D. M. (1973). Free energies of imperfect nucleic acid helices III. Small internal loops resulting from mismatches. *J. Mol. Biol.* **78,** 301–309.

Griffiths-Jones, S., Bateman, A., Marshall, M., Kharna, A., and Eddy, S. R. (2003). Rfam: An RNA family database. *Nucleic Acids Res.* **31,** 439–441.

Griffiths-Jones, S., Moxon, S., Marshall, M., Kharna, A., Eddy, S. R., and Bateman, A. (2005). Rfam: Annotating non-coding RNAs in complete genomes. *Nucleic Acids Res.* **33,** D121–D124.

Hammes, G. G. (1974). Temperature-jump methods. *In* "Techniques of Chemistry, Vol. 6," (G. G. Hammes, ed.), Wiley-Interscience New York.

He, L., Kierzek, R., SantaLucia, J. Jr., Walter, A. E., and Turner, D. H. (1991). Nearest-neighbor parameters for GU mismatches. *Biochemistry* **30,** 11124–11132.

Holbrook, J., Capp, M., Saeker, R., and Record, M. T. Jr. (1999). Enthalpy and heat capacity changes for formation of an oligomeric DNA duplex: Interpretation in terms of coupled processes of formation and association of single-stranded helices. *Biochemistry* **38,** 8409–8422.

Kierzek, R., Burkard, M. E., and Turner, D. H. (1999). Thermodynamics of single mismatches in RNA duplexes. *Biochemistry* **38,** 14214–14223.

Marky, L. A., and Breslauer, K. J. (1987). Calculating thermodynamic data for transitions of any molecularity from equilibrium melting curves. *Biopolymers* **26,** 1601–1620.

Mathews, D. H., Sabina, J., Zuker, M., and Turner, D. H. (1999). Expanded sequence dependence of thermodynamic parameters improves prediction of RNA secondary structure. *J. Mol. Biol.* **288,** 911–940.

Mathews, D. H., Disney, M. D., Childs, J. L., Schroeder, S. J., Zuker, M., and Turner, D. H. (2004). Incorporating chemical modification constraints into a dynamic programming algorithm for prediction of RNA secondary structure. *Proc. Natl. Acad. Sci. USA* **101,** 7287–7292.

McDowell, J. A., and Turner, D. H. (1996). Investigation of the structural basis for thermodynamic stabilities of tandem GU mismatches: Solution structure of (rGAG-GUCUC)2 by two-dimensional NMR and simulated annealing. *Biochemistry* **35,** 14077–14089.

Mergny, J.-L., Li, J., Lacroix, L., Amrane, S., and Chaires, J. B. (2005). Thermal difference spectra: A specific signature for nucleic acid structures. *Nucleic Acids Res.* **33,** e138.

Mikulecky, P., and Feig, A. (2006). Heat capacity changes associated with nucleic acid folding. *Biopolymers* **82,** 38–58.

Miller, S., Jones, L. E., Giovannitti, K., Piper, D., and Serra, M. J. (2008). Thermodynamic analysis of 5' and 3' single- and 3' double nucelotide overhangs neighboring wobble terminal base pairs. *Nucleic Acids Res.* **36,** 5652–5659.

Miyoshi, D., Nakamura, K., Tateishi-Karimata, H., Ohmichi, T., and Sugimoto, N. (2009). Hydration of Watson–Crick base pairs and dehydration of Hoogsteen base pairs inducing structural polymorphism under molecular crowding conditions. *J. Am. Chem. Soc.* **131,** 3522–3531.

Narlikar, G., Kosla, M., Usman, N., and Herschlag, D. (1997). Quantitating tertiary binding energies of 2'OH groups on the P1 duplex of the *Tetrahymena* ribozyme: Intrinsic binding energy in an RNA enzyme. *Biochemistry* **36,** 2465–2477.

Ogle, J., Murphy, F., Tarry, M., and Ramakrishnan, V. (2002). Selection of tRNA by the ribosome requies a transition from an open to a closed form. *Cell* **111,** 721–732.

O'Toole, A. S., Miller, S., and Serra, M. J. (2005). Stability of 3' double nucleotide overhangs that model the 3' ends of siRNA. *RNA* **11,** 512–516.

O'Toole, A. S., Miller, S., Haines, N., Zink, M. C., and Serra, M. J. (2006). Comprehensive thermodynamic analysis of 3' double nucleotide overhangs neighboring Watson–Crick terminal base pairs. *Nucleic Acids Res.* **34,** 3338–3344.

Palmenberg, A., Spiro, D., Kuzmickas, R., Wang, S., Djikeng, A., Rather, J., Fraser-Liggett, C., and Liggett, S. (2009). Sequencing and analyses of all known human rhinovirus genomes reveal structure and evolution. *Science* **324,** 55–59.

Parisien, M., and Major, F. (2008). The MC-Fold and MC-Sym pipeline infers RNA structure from sequence data. *Nature* **452,** 51–55.

Petersheim, M., and Turner, D. H. (1983). Base-stacking and base-pairing contributions to helix stability: Thermodynamics of double-helix formation with CCGG, CCGGp, CCGGAp, ACCGGp, CCGGUp, and ACCGGUp. *Biochemistry* **22,** 256–263.

Pyle, A. M., Moran, S., Strobel, S. A., Chapman, T., Turner, D. H., and Cech, T. R. (1994). Replacement of the conserved GU with a GC pair at the cleavage site of the *Tetrahymena* ribozyme decreases binding reactivity and fidelity. *Biochemistry* **33,** 13856–13863.

SantaLucia, J. Jr., Kierzek, R., and Turner, D. H. (1991). Stabilities of consecutive A·C, C·C, G·G, U·C, and U·U mismatches in RNA internal loops: Evidence for stable hydrogen-bonded U·U and $C \cdot C^{+}$ pairs. *Biochemistry* **30,** 8242–8251.

SantaLucia, J. Jr., and Turner, D. H. (1997). Measuring the thermodynamics of RNA secondary structure formation. *Biopolymers* **44,** 309–319.

SantaLucia, J. Jr., Allawi, H. T., and Seneviratne, P. A. (1996). Improved nearest-neighbor parameters for predicting DNA duplex stability. *Biochemistry* **35,** 3555–3562.

Schroeder, S. J., and Turner, D. H. (2000). Factors affecting the thermodynamic stability of small asymmetric internal loops in RNA. *Biochemistry* **39,** 9257–9274.

Schroeder, S. J., and Turner, D. H. (2001). Thermodynamic stabilities of internal loops with GU closing pairs in RNA. *Biochemistry* **40,** 11509–11517.

Siegfried, N. A., and Bevilacqua, P. C. (2009). Thinking inside the box: designing, implementing, and interpreting thermodynamic cycles to dissect cooperativity in RNA and DNA folding. *Methods Enzymol.* **455,** 365–393.

Sugimoto, N., Nakano, S., Yoneyama, M., and Honda, K. (1996). Improved thermodynamic parameters and helix initiation factor to predict stability of DNA duplexes. *Nucleic Acids Res.* **24,** 4501–4505.

Testa, S. M., and Gilham, P. T. (1993). Analysis of oligonucleotide structure using hyperchromism measurements at long wavelengths. *Nucleic Acids Res.* **21,** 3907–3908.

Turner, D. H. (1986). Temperature jump methods. *In* "Techniques of Chemistry, Vol. 6," (C. Bernasconi, ed.), Wiley-Interscience, New York.

Turner, D. H. (2000). Conformational changes. *In* "Nucleic Acids: Structures, Properties, and Functions," (V. A. Bloomfield, D. M. Crothers, and I. Tinoco Jr., eds.) pp. 259–334. University Science Books, Sausalito, CA.

Uzilov, A. V., Keegan, J. M., and Mathews, D. H. (2006). Detection of non-coding RNAs on the basis of predicted secondary structure formation free energy change. *BMC Bioinformatics* **7,** 173–203.

Walter, A. E., Wu, M., and Turner, D. H. (1994). The stability and structure of tandem GA mismatches in RNA depend on closing base pairs. *Biochemistry* **33,** 11349–11354.

Washietl, S., Hofacker, I. L., and Stadler, P. F. (2005). Fast and reliable prediction of noncoding RNAs. *Proc. Natl. Acad. Sci. USA* **102,** 2454–2459.

Wilkinson, K. A., Gorelick, R. J., Vasa, S. M., Guex, N., Rein, A., Mathews, D. H., Giddings, M. C., and Weeks, K. M. (2008). High-throughput SHAPE analysis reveals structures in HIV-1 genomic RNA strongly conserved across distinct biological states. *PLoS Biol.* **6,** e96.

Wu, M., and Turner, D. H. (1996). Solution structure of r(GCGGACGC)2 by two-dimensional NMR and the iterative relaxation matrix approach. *Biochemistry* **35,** 9677–9689.

Xia, T., SantaLucia, J. Jr., Burkard, M. E., Kierzek, R., Schroeder, S. J., Jiao, X., Cox, C., and Turner, D. H. (1998). Thermodynamic parameters for an expanded nearest-neighbor model for formation of RNA duplexes with Watson–Crick base pairs. *Biochemistry* **37,** 14719–14735.

Zuker, M. (1989). On finding all suboptimal foldings of an RNA molecule. *Science* **244,** 48–52.